

Direct observation of electron emission from the grain boundaries of chemical vapour deposition diamond films by tunneling atomic force microscopy

Vijay Chatterjee, Robert Harniman, Paul W. May, and P. K. Barhai

Citation: [Applied Physics Letters](#) **104**, 171907 (2014); doi: 10.1063/1.4875059

View online: <http://dx.doi.org/10.1063/1.4875059>

View Table of Contents: <http://scitation.aip.org/content/aip/journal/apl/104/17?ver=pdfcov>

Published by the [AIP Publishing](#)

Articles you may be interested in

[Influence of grain boundary on electrical properties of organic crystalline grains investigated by dual-probe atomic force microscopy](#)

Appl. Phys. Lett. **103**, 173109 (2013); 10.1063/1.4826582

[Modelling of infrared optical constants for polycrystalline low pressure chemical vapour deposition ZnO:B films](#)

J. Appl. Phys. **113**, 123104 (2013); 10.1063/1.4795809

[The effect of hydrogen desorption kinetics on thermionic emission from polycrystalline chemical vapor deposited diamond](#)

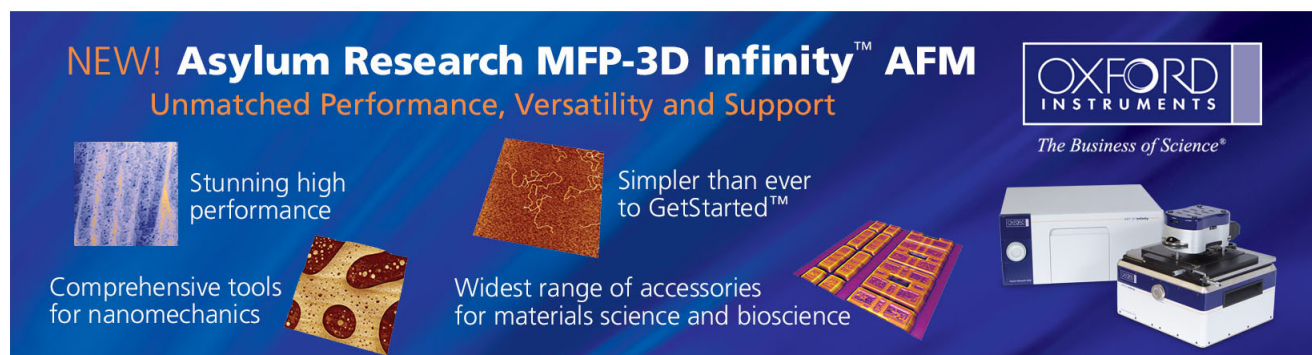
Appl. Phys. Lett. **101**, 243509 (2012); 10.1063/1.4772069

[Direct observation of preferential heating near grain boundaries in patterned silicide films](#)

J. Appl. Phys. **108**, 063539 (2010); 10.1063/1.3475506

[Direct observation of electron emission site on boron-doped polycrystalline diamond thin films using an ultra-high-vacuum scanning tunneling microscope](#)

Appl. Phys. Lett. **75**, 3219 (1999); 10.1063/1.125283

The advertisement features a dark blue background with white and orange text. At the top left, it reads 'NEW! Asylum Research MFP-3D Infinity™ AFM' in large white letters, followed by 'Unmatched Performance, Versatility and Support' in orange. On the right, the Oxford Instruments logo is shown with the tagline 'The Business of Science®'. Below the text are four images: a blue textured surface, a brown textured surface, a yellow and red patterned surface, and a photograph of the AFM instrument. Text descriptions are placed around these images: 'Stunning high performance' next to the blue surface, 'Simpler than ever to GetStarted™' next to the brown surface, 'Comprehensive tools for nanomechanics' next to the yellow and red surface, and 'Widest range of accessories for materials science and bioscience' next to the instrument photo.

Direct observation of electron emission from the grain boundaries of chemical vapour deposition diamond films by tunneling atomic force microscopy

Vijay Chatterjee,^{1,2} Robert Harniman,¹ Paul W. May,^{1,a)} and P. K. Barhai²

¹*School of Chemistry, University of Bristol, Cantock's Close, Bristol BS8 1TS, United Kingdom*

²*Department of Physics, Birla Institute of Technology, Mesra, Ranchi 835215, India*

(Received 27 March 2014; accepted 24 April 2014; published online 2 May 2014)

The emission of electrons from diamond in vacuum occurs readily as a result of the negative electron affinity of the hydrogenated surface due to features with nanoscale dimensions, which can concentrate electric fields high enough to induce electron emission from them. Electrons can be emitted as a result of an applied electric field (field emission) with possible uses in displays or cold-cathode devices. Alternatively, electrons can be emitted simply by heating the diamond in vacuum to temperatures as low as 350 °C (thermionic emission), and this may find applications in solar energy generation or energy harvesting devices. Electron emission studies usually use doped polycrystalline diamond films deposited onto Si or metallic substrates by chemical vapor deposition, and these films have a rough, faceted morphology on the micron or nanometer scale. Electron emission is often improved by patterning the diamond surface into sharp points or needles, the idea being that the field lines concentrate at the points lowering the barrier for electron emission. However, there is little direct evidence that electrons are emitted from these sharp tips. The few reports in the literature that have studied the emission sites suggested that emission came from the grain boundaries and not the protruding regions. We now present direct observation of the emission sites over a large area of polycrystalline diamond using tunneling atomic force microscopy. We confirm that the emission current comes mostly from the grain boundaries, which is consistent with a model for emission in which the non-diamond phase is the source of electrons with a threshold that is determined by the surrounding hydrogenated diamond surface.

© 2014 AIP Publishing LLC. [<http://dx.doi.org/10.1063/1.4875059>]

Chemical vapor deposition (CVD) diamond films are excellent materials for use as electron field emitters due to their low or negative electron affinity (NEA), which lowers the effective barrier that electrons need to overcome to escape from the surface into vacuum.¹ Moreover, diamond has excellent mechanical and chemical properties, including high hardness, high thermal conductivity, and compatibility with silicon fabrication processes, that make it a potential candidate for a range of vacuum microelectronic devices, such as high-power switches, electron sources for microwave (MW) tubes, large-area electron guns for high-definition television, and high-speed, high-power amplifiers, and integrated circuits.² Recently, it was reported that by putting a thin CVD diamond coating onto vertically aligned carbon nanotube (CNT) “teepee” structures, the lifetime of field emission devices could be greatly extended such that these structures might be used as field emitter arrays in commercial flat-panel displays.³

Despite this, the mechanism for electron emission from diamond remains somewhat controversial. Field emission follows the Fowler-Nordheim equation (1) for electron emission via quantum mechanical tunneling through a potential barrier⁴

$$J(E) = \frac{A(\beta E)^2}{\phi} \exp\left(-\frac{b\phi^3}{\beta E}\right) \quad (1)$$

where J is the emission current density in $\text{A } \mu\text{m}^{-2}$, $b = 6.83 \times 10^3 \text{ eV}^{-3/2} \text{ V } \mu\text{m}^{-1}$, $A = 1.56 \times 10^{-6} \text{ A V}^{-2} \text{ eV}$, E is the applied electric field in $\text{V } \mu\text{m}^{-1}$, and ϕ is the work function of the material in eV. The field enhancement factor, β , is usually interpreted as a geometrical effect due to sharp points or edges which concentrate the electric field. Many workers have gone to considerable effort to process diamond into cones, needles or sharpened structures in order to increase the β value and thereby improve the emission efficiency.¹ However, values for β measured from diamond and other carbon surfaces are often several 1000 or more, which are much larger than the theoretical values of 10–100 typically possible by consideration of geometrical effects alone. Furthermore, field emission studies using CNTs have shown that short, stubby CNTs⁵ or even exceptionally short CNTs⁶ emit electrons much better than longer ones, again, in violation of conventional ideas.

As a result, a number of other explanations have been proposed for the observed field enhancement. Geis and co-workers⁷ suggested that the field enhancement occurs at the metal-diamond-vacuum triple junction where the diamond film, substrate and vacuum meet. Electrons tunnel from the substrate into diamond surface states, where they are accelerated to energies sufficient to be ejected into vacuum, usually

^{a)}Electronic mail: paul.may@bristol.ac.uk

traveling up through grain boundaries or up the sides of diamond grains. However, this mechanism does not explain enhanced field emission from very thick diamond films where the field at the base of the film is very small, or from freestanding diamond films where there is no substrate.

It is known that a hydrogenated diamond surface is necessary to obtain high electron yields,⁸ but electron emission also correlates with the number and density of grain boundaries containing non-diamond *sp*² carbon.⁹ To account for this, Cui and co-workers¹⁰ devised a model in which the lowering of the emission threshold is due to a reduction of the electron affinity of the diamond surface surrounding graphitic structures on the surface, such as grain boundaries. In this case, electron emission takes place from the graphitic phase, whereas the emission barrier is controlled by the surrounding diamond matrix. Robertson¹¹ and Ilie *et al.*¹² proposed a similar model to explain enhanced field emission from other forms of carbon films, including flat, smooth diamondlike carbon. Some experimental evidence supports these models. Field emission was shown to be enhanced when a diamond surface was covered with patches of nanoscale graphitic impurities,¹³ and undoped polycrystalline diamond particles deposited on a Si surface exhibited electron emission at relatively low turn-on fields (0.8–2.0 V μm^{-1}), whereas no emission was observed from their single-crystalline counterparts. Miyamoto and co-workers¹⁴ showed that electron dynamics strongly affects the emission efficiency depending on the potential profile at the surface. It was recently demonstrated that ultrananocrystalline diamond (UNCD) films on a flat surface with appropriate amount of nitrogen incorporated in grain boundaries also exhibit low threshold electric fields, indicating that atomic-scale grain boundaries may concentrate electric fields as efficiently or even more so than sharp features.¹⁵ Circumstantial evidence that electron emission arises from grain boundaries was provided by May and co-workers¹⁶ who deliberately used excessive bias to burn out the emission sites in polycrystalline diamond films. Investigation of the damage sites showed ring-like craters surrounding grains, suggesting that the grain boundary, not the grain or the tip of the grain, had been eroded due to passage of excessive current. Direct evidence, however, for grain boundary emission has proven elusive. One technique, field electron emission microscopy (FEEM), has been developed which can collect the field-emitted electrons and image them enabling their origin to be determined. However, FEEM has proven difficult to implement on diamond, and results have been inconclusive. Garguilo and co-workers¹⁷ used FEEM to study the emitting sites from nanocrystalline diamond (NCD) films and found that the emission originated from localized regions smaller than 100 nm in size. The authors concluded that along with grain boundary emission there must be some additional unexplained emission mechanisms at work.

Arguably, the most convincing direct evidence to date comes from three reports which describe the use of scanning tunneling microscopy (STM) to map simultaneously the field emission intensity and morphology of diamond films. Karabutov and co-workers¹⁸ used STM to study a microcrystalline diamond film and showed that emission sites were not associated with sharp tips, but instead with the valleys

between grains. However, due to the difficult nature of the experiment, data for only one sample at 400 \times 400 nm resolution was presented. Sankaran and co-workers¹⁹ used a similar high resolution STM technique on Cu-doped UNCD films, and also showed that the grain boundaries were preferred emission sites. They reported that I-V emission characteristics were much superior from the grain boundaries compared to those from the grains. However, these studies were limited to Cu-doped UNCD, so extrapolating the findings to other, less defective forms of diamond, might not be appropriate. One of the first, and most detailed, studies in this area was performed by Krauss and co-workers in 2001,²⁰ who used a metal-coated atomic force microscopy (AFM) tip in contact with the surface of a UNCD-coated Si micro-emitter to measure the film topography, and then applied electric fields while using the AFM tip as an STM to measure the electron emission at different locations. This work revealed that the electron emission was related to minima or inflection points in the surface topography, and not to surface asperities. These authors concluded that the grain boundaries provided a conducting path from the substrate to the surface, and enhanced both the local electric field via internal structures rather than surface topography, and the local density of states within the bulk diamond band gap.

Advances in STM and AFM over the past few years have seen the development of this conducting-AFM/STM combination into a highly sensitive technique called tunneling atomic force microscopy²¹ (TUNA—the acronym is the official designation for this process by the equipment manufacturers, Bruker). This allows a tunneling current to be obtained from a sharpened tip attached to a cantilever, while simultaneously the tip traverses across the sample surface tracking height and morphological information. Whilst standard STM requires sample surfaces to be smooth on the nanometer scale, the physical tracking of topography in TUNA means that samples with a surface r.m.s. roughness of several microns can be investigated over scan areas up to hundreds of square microns. This allows a wider picture of the overall morphology to be obtained. Physical tracking also means that, unlike the constant-current mode of STM, the height data collected via deflection of the cantilever beam avoids possible artefacts introduced by variations in the conductivity of the sample surface. Another major advantage of TUNA is that it has very high current sensitivity with a current measurement range up to 120 pA with a noise level of 50 fA, which is particularly useful for the electrical characterisation of low-conductivity samples at high lateral resolution. It must be emphasized that TUNA is *not* the same as conducting AFM, where the tip remains in contact with the sample for all measurements. In TUNA, to obtain field emission currents, as opposed to just surface conductivity, the topography is first scanned in contact mode but then the tip is withdrawn from the surface a distance of \sim 1 nm using a sensitive feedback system known as PeakForce control, and then the surface is rescanned again maintaining this constant tip height.

Three types of diamond film were investigated with varying surface morphologies. They were all deposited in a CVD reactor using methane/hydrogen gas mixtures but under different process conditions leading to polycrystalline

diamond films with different grain sizes. The films consisted of (i) microcrystalline diamond (MCD) faceted crystallites of size $\sim 1 \mu\text{m}$, (ii) NCD-400 rounded crystallites of size $\sim 400 \text{ nm}$, and (iii) NCD-30, rounded crystallites of size $10\text{--}50 \text{ nm}$ (averaging $\sim 30 \text{ nm}$).

A first set of diamond films was grown using a 1 cm^2 Si (100) substrate that had been pre-seeded by spraying it with a suspension of $5\text{--}10 \text{ nm}$ nanodiamond in methanol. Deposition occurred at 20 torr in a hot filament reactor using standard CVD conditions.²² The gas mixture used was 1% CH_4 in H_2 for MCD, 4% CH_4 in H_2 for NCD-400, and 1% $\text{CH}_4 + 1\% \text{ H}_2$ in Ar for NCD-30. The rhenium filament (2400 K) was placed 3 mm above the surface of the heated substrate ($\sim 900^\circ\text{C}$). Film thicknesses were $4 \mu\text{m}$, $4.5 \mu\text{m}$, and $1.5 \mu\text{m}$, respectively, for MCD, NCD-400, and NCD-30.

A second set of diamond films was grown on a 1 cm^2 polished aluminium nitride substrate which was pre-seeded, as above. CVD occurred in a 1 kW MW plasma reactor for 1 h with process conditions ($\text{H}_2\%$, $\text{CH}_4\%$, $\text{Ar}\%$, $\text{N}_2\%$, pressure in torr): MCD (88.5, 4.5, 7, 0, 125); NCD-400 (92.75, 6.5, 0, 0.75, 110); and NCD-30 (9.9, 0.6, 89.5, 0, 170), leading to films of thickness 0.45 , 0.35 , and $0.4 \mu\text{m}$ (all $\pm 0.05 \mu\text{m}$), respectively. Due to AlN 's smooth polished surface and its thermal expansion mismatch with diamond, upon cooling after CVD the diamond film delaminated from the substrate as a freestanding sheet which could be manipulated with tweezers.

A third set of diamond films was grown in a hot filament reactor with conditions identical to those for the first set, given above, except with 10 000 ppm diborane gas added to the gas mixture. These boron-doped diamond films had boron concentrations $\sim 3 \times 10^{20} \text{ cm}^{-3}$ (based on previously calibrated SIMS measurements) and exhibited metallic conductivity.

TUNA was performed utilising a Bruker Multi-mode V AFM in ambient conditions in both contact mode for topology and using PeakForce control for field emission measurements at a tip height of $\sim 1 \text{ nm}$. The bases of the diamond films were attached to a steel disc using conductive silver paint (G3790 Agar Scientific) for the purpose of creating a bias between the sample and the AFM tip. The conductivity of the cantilevers was provided by a 20 nm platinum-iridium coating to the front and backside of the lever, giving a nominal tip radius of 20 nm (SCM-PIC; Bruker, California, USA). Precautions were taken to ensure that both the roughness and hardness of the diamond samples did not cause excess wear to the tip and risk damage to the conducting Pt-Ir layer. First, low force regimes were maintained, not exceeding 3 nN, to reduce the effect of normal forces. Maintaining low tip velocities between 125 nm s^{-1} and $2.5 \mu\text{m s}^{-1}$ enabled the feedback control to maintain a stable scan regime, reliably tracking the larger topographic features of the sample. In addition, very low bias potentials between the tip and sample were used, typically in the range of a few hundred mV, to keep current flow below 200 pA, thus avoiding melting of the tip's conductive coating. After data collection, the cantilever tip was checked via SEM and a tip calibration grid and showed negligible wear, with the tip radius remaining in the region of 20 nm.

In order to confirm that the measured tunneling current was a true reflection of the emission properties of the surface and not simply an artefact of surface topology, a number of tests were performed. Scans were repeated in four different directions to check that the data from each scan were all in good agreement. This confirmed that the additional emission observed on the sides of grains measured at the base of a valley was not due to tracking errors. To check for tip convolution effects, the relative aspect ratio of the tip and those of the surface features were measured in a high resolution SEM. The back and front sides of the tetrahedral cantilever tip displayed angles between 15° and 25° to the normal, respectively. The highest average aspect ratio of the samples was for MCD, with values $\sim 40^\circ$ from the normal to the sample plane. The ratio of these values means that the 20 nm tip penetrated between grains down to the grain boundary as close as the tip radius allowed. Comparison to SEM images confirmed that the topographic data collected was not convoluted by the tip shape, because the grains displayed a pronounced 4-sided pyramid structure regardless of the tetrahedral tip. Nevertheless, a greater tip interaction area was presented to the sample within the valleys which could result in an increased current flow. Upon increasing the bias potential between the tip and the sample, the intensity of current measured from the valleys increased as expected. However, no new current was detected from the peaks of the grains as the voltage increased, indicating that the contrast between very strong current measured in the valleys and the lack of strong current at the grain peaks was not a geometric effect of the tip, but an innate difference in the emission properties of the grain peaks and the grain boundaries.

TUNA data from these three types of film can be seen in Fig. 1. It is clear that as the number of crystallites and grain boundaries increases, so do the number and density of emission sites, consistent with previous reports.⁹

In the 3D isometric images shown in Fig. 2, it is clear that there is an enhancement of the emission current from the valleys between the crystals where the grain boundaries reside, and not from the protruding edges or tips.

The measurements were repeated using freestanding MCD and NCD-400, and the results again showed that the tunneling currents were greatest at the grain boundaries. The fact that this set of films had no substrate effectively rules out Geis' triple-junction model⁷ for field emission in these samples.

The TUNA image from the B-doped MCD film is shown in Fig. 3. Again, the grain boundaries show the enhanced tunneling current, but now the emission region extends for a few 100 nm either side of the grain boundary. This is also consistent with Cui and co-workers' model¹⁰ for field emission in that the conducting surface will allow the reduced work function near the grain boundaries to spread out.

Care needs to be taken in interpreting these results as the field emission processes in TUNA are not identical to those in standard field emission experiments, or in direct measurements such as those using FEEM.¹⁷ In TUNA, the tunneling is direct, i.e., from the surface through a 1 nm air gap into the tip and is therefore strongly dependent upon the tip-sample separation, whereas in standard field emission the tunneling is from the surface into the vacuum and is

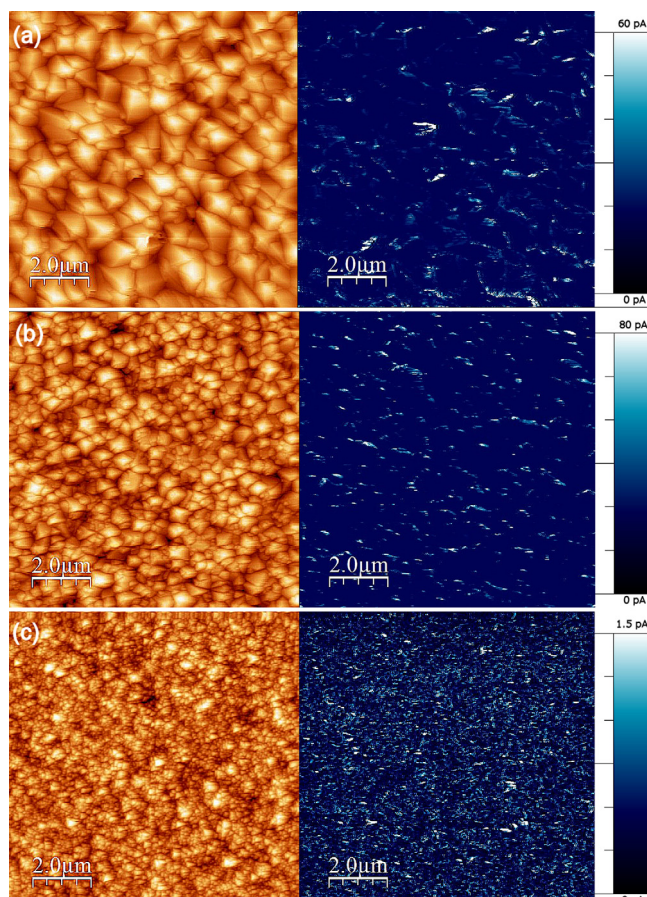


FIG. 1. $10\ \mu\text{m} \times 10\ \mu\text{m}$ TUNA images of freestanding films of: (a) MCD (sample bias 0.1 V), (b) NCD-400 (sample bias 1 V), and (c) NCD-30 (sample bias 4.5 V). The left-hand image shows the surface topography measured using the AFM tip. The right-hand image shows the tunneling current from the same region with the color scale for the tip current after it was withdrawn a distance of $\sim 1\ \text{nm}$.

dependent upon the local field strength and not the tip-sample distance—although this effectively sets the local field strength. Nevertheless, we propose that the two mechanisms are sufficiently similar that the TUNA measurements are

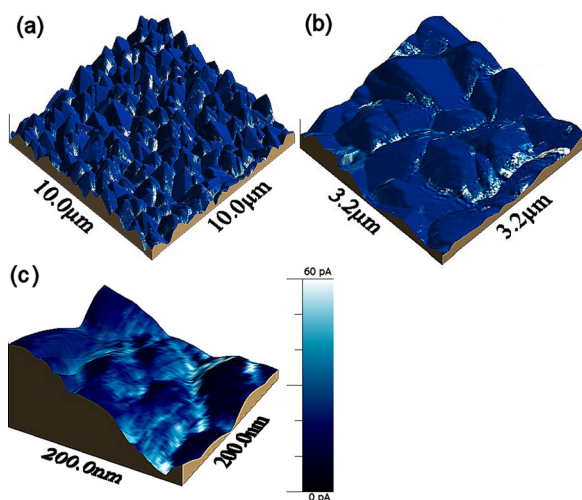


FIG. 2. 3D projections of the TUNA topographic data for a freestanding MCD film with the tunneling current superimposed. The sample potentials used and current scale are the same as in Fig. 1(a). (a) MCD: $10\ \mu\text{m} \times 10\ \mu\text{m}$ image $\times 0.89\ \mu\text{m}$, (b) MCD: $3.2\ \mu\text{m} \times 3.2\ \mu\text{m} \times 0.7\ \mu\text{m}$, and (c) MCD: $0.2\ \mu\text{m} \times 0.2\ \mu\text{m} \times 0.12\ \mu\text{m}$.

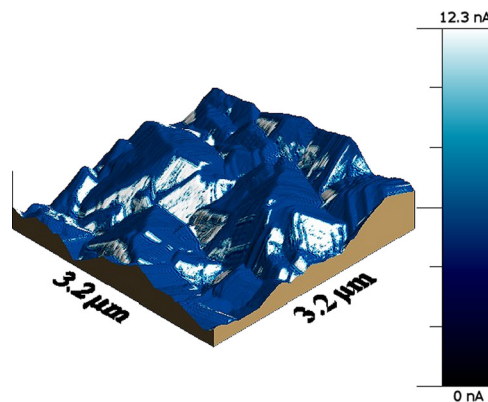


FIG. 3. 3D projection of the TUNA topographic data for a B-doped MCD film with the tunneling current superimposed (sample bias 0.1 V). The scale is $3.2\ \mu\text{m} \times 3.2\ \mu\text{m} \times 0.8\ \mu\text{m}$.

representative of the preferred field emission sites in diamond—although we accept opinions may differ on this point.

In conclusion, this study has provided direct evidence that electron field emission from diamond films originates preferentially from the grain boundaries in undoped and p-type polycrystalline diamond films with grain sizes down to $\sim 10\ \text{nm}$. This is consistent with the model for electron field emission based on lowering of the emission threshold due to a reduction of the electron affinity of the diamond surface surrounding graphitic structures on the surface and confirms the initial findings of previous groups.^{18–20} Work is currently underway to determine if field emission from n-type (phosphorus- or nitrogen-doped) diamond films behaves in the same way. Nevertheless, we suggest that it may be advantageous to design diamond field emission devices using fine-grained diamond, such as NCD or UNCD, and the expense and fabrication problems of patterning the diamond into sharp tips or needles may be unnecessary. This finding may be of benefit to studies of thermionic emission also, since the thermionic emission current depends strongly upon the local surface work function, which can be affected by the presence of grain boundaries. Modifying the TUNA system to enable the study of hot substrates (up to $500\ ^\circ\text{C}$) might be an interesting suggestion.

The authors wish to thank the UK Commonwealth Commission for funding V.C. for his year in the UK. We also wish to thank Oliver Fox for depositing the MW CVD diamond samples on AlN, and to Kane O'Donnell for useful discussions about field emission mechanisms. The authors also thank the Electron Microscopy and Scanning Probe Microscopy Unit of the School of Chemistry, University of Bristol for use of their equipment and help with the TUNA system.

¹J. L. Davidson, W. P. Kang, K. Subramanian, and Y. M. Wong, *Philos. Trans. R. Soc., A* **366**, 281 (2008).

²K. Subramanian, W. P. Kang, J. L. Davidson, N. Ghosh, and K. F. Galloway, *Microelectron. Eng.* **88**, 2924 (2011).

³Y. Zou, P. W. May, S. M. C. Vieira, and N. A. Fox, *J. Appl. Phys.* **112**, 044903 (2012).

⁴G. Chen, S. Neupane, W. Li, L. Chen, and J. Zhang, *Carbon* **52**, 468 (2013).

⁵M. Chhowalla, C. Ducati, N. L. Rupasinghe, K. B. K. Teo, and G. A. J. Amaratunga, *Appl. Phys. Lett.* **79**, 2079 (2001).

- ⁶C. J. Shearer, J. G. Shapter, J. S. Quinton, P. C. Dastoor, L. Thomsen, and K. M. O'Donnell, *J. Mater. Chem.* **18**, 5753 (2008).
- ⁷M. W. Geis, N. N. Efremow, K. E. Krohn, J. C. Twichell, T. M. Lyszczarz, R. Kalish, J. A. Greer, and M. D. Tabat, *Nature* **393**, 431 (1998).
- ⁸J. B. Cui, J. Ristein, M. Stammler, K. Janischowsky, G. Kleber, and L. Ley, *Diamond Relat. Mater.* **9**, 1143 (2000).
- ⁹D. Pradhan and I. N. Lin, *ACS Appl. Mater. Interfaces* **1**, 1444 (2009).
- ¹⁰J. B. Cui, J. Ristein, and L. Ley, *Phys. Rev. B* **60**, 16135 (1999).
- ¹¹J. Robertson, *J. Vac. Sci. Technol., B* **17**, 659 (1999).
- ¹²A. C. Ilie, A. C. Ferrari, T. Yagi, S. E. Rodil, J. Robertson, E. Barborini, and P. Milani, *J. Appl. Phys.* **90**, 2024 (2001).
- ¹³J. B. Cui and J. Robertson, *J. Vac. Sci. Technol., B* **20**, 238 (2002).
- ¹⁴Y. Miyamoto, T. Miyazaki, D. Takeuchi, H. Okushi, and S. Yamasaki, *Appl. Phys. Lett.* **103**, 123104 (2013).
- ¹⁵S. A. Getty, O. Auciello, A. V. Sumant, X. Wang, D. P. Galvin, and P. R. Mahaffy, *Proc. SPIE* **7679**, 76791N-1 (2010).
- ¹⁶P. W. May, S. Höhn, M. N. R. Ashfold, W. N. Wang, N. A. Fox, T. J. Davis, and J. W. Steeds, *J. Appl. Phys.* **84**, 1618 (1998).
- ¹⁷J. M. Garguilo, F. A. M. Köck, B. Brown, and R. J. Nemanich, in *Proceedings of Sixth Applied Diamond Conference/Second Frontier Carbon Technology Joint Conference* (2001), p. 133.
- ¹⁸A. V. Karabutov, V. D. Frolov, S. M. Pimenov, and V. I. Konov, *Diamond Relat. Mater.* **8**, 763 (1999).
- ¹⁹K. J. Sankaran, K. Panda, B. Sundaravel, N. H. Tai, and I. N. Lin, *J. Appl. Phys.* **115**, 063701 (2014).
- ²⁰A. R. Krauss, O. Auciello, M. Q. Ding, D. M. Gruen, Y. Huang, V. V. Zhirnov, E. I. Givargizov, A. Breskin, R. Chechen, E. Shefer, V. Konov, S. Pimenov, A. Karabutov, A. Rakhimov, and N. Suetin, *J. Appl. Phys.* **89**, 2958 (2001).
- ²¹V. Yanef, M. Rommel, M. Lemberger, S. Petersen, B. Amon, T. Erbacher, A. J. Bauer, H. Ryssel, A. Paskaleva, W. Weinreich *et al.*, *Appl. Phys. Lett.* **92**, 252910 (2008).
- ²²P. W. May, *Philos. Trans. R. Soc., A* **358**, 473 (2000).